Towards a Self-contained Soft Robotic Fish: On-Board Pressure Generation and Embedded Electro-permanent Magnet Valves

Andrew D. Marchese, Cagdas D. Onal, and Daniela Rus

Abstract. This paper details the design, fabrication and experimental verification of a complete, tetherless, pressure-operated soft robotic platform. Miniature CO_2 cartridges in conjunction with a custom pressure regulating system are used as an on-board pressure source and embeddable electro-permanent magnet (EPM) [9] valves [13] are used to address supporting hardware requirements. It is shown that this system can repeatedly generate and regulate supply pressure while driving a fluidic elastomer actuator (FEA) [7, 14, 13]. To demonstrate our approach in creating tetherless soft mobile robots, this paper focuses on an example case-study: a soft robotic fish. An underactuated propulsion system emulating natural caudal fin and peduncle movement is designed, fabricated, and subsequently experimentally characterized.

1 Introduction

One key requirement in creating robots that are integral parts of our daily lives is body elasticity. Elasticity is a form of intelligence embedded within the mechanics of a robot body. A soft robot is inherently safe and adaptive. It can deform and absorb energy in case of a collision [1]. Environmental uncertainty is less of a problem, reducing complexity in modeling, planning, and control. Soft robots have many potential applications [20], including bio-inspired robotics [6].

Among alternatives, fluid pressure is a suitable actuation method for soft robots. This form of mechanical energy induces stresses directly inside an elastomer [21], to enable a large actuation range, limited only by the mechanical strength of the

Andrew D. Marchese · Cagdas D. Onal · Daniela Rus
Computer Science and Artificial Intelligence Laboratory,
Massachusetts Institute of Technology, 32 Vassar St. Cambridge, MA 02139, USA
e-mail: {andy,cagdas,rus}@csail.mit.edu

Cagdas D. Onal
Department of Mechanical Engineering, Worcester Polytechnic Institute,
100 Institute Road, Worcester, Massachusetts 01609
e-mail: cdonal@wpi.edu

J.P. Desai et al. (Eds.): *Experimental Robotics*, STAR 88, pp. 41–54.
DOI: 10.1007/978-3-319-00065-7_4

material. We build our robots relying on a novel actuator technology, tagged as fluidic elastomer actuators (FEAs) [7, 14, 13]. FEAs use synthetic elastomer films as pneumatic or hydraulic bending elements. They are operated by the expansion of embedded fluidic channels under pressure input.

This family of soft robots has a unique set of challenges. A fluidic actuation principle requires a pressure source [8] for operation, which limits mobility and mainstream usage. For mobile applications, these robots need to generate the actuator supply pressure on-board. Furthermore, to address, pressurize, and depressurize actuators, this class of robots requires a valve array, which can occupy considerable real-estate and be cumbersome to install on-board. In order to create completely tetherless fluid-powered soft robots, actuator supply pressure and control valves must be moved on-board. To date, the authors are aware of only a single system [14] that accomplishes this task.

Building on our previous results, this paper presents a complete, tetherless, pressure-operated soft robotic platform by addressing both challenges: (1) We use miniature CO_2 cartridges with custom pressure regulating systems as on-board pressure sources; and (2) we use a new, embeddable, and energy-efficient electro-permanent magnet (EPM) [9] valve [13] to address supporting valve requirements.

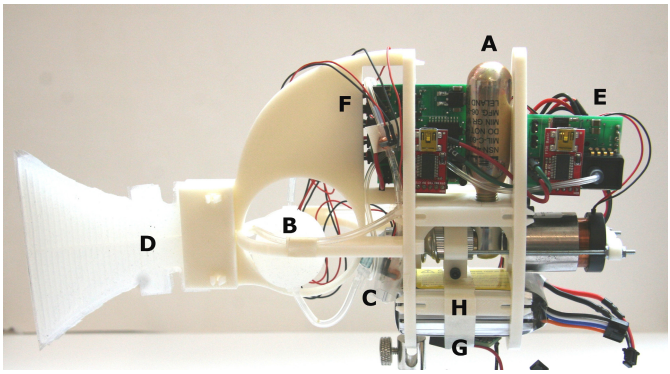

Fig. 1 Fish prototype realized with fluidic actuation system. The system is composed of (A) CO_2 storage and release mechanism, (B) elastic reservoir vessel, (C) embeddable electro-permanent magnet (EPM) valves [13], (D) fluidic elastomer actuator [7, 14, 13], (E) custom CO_2 regulator board, (F) custom EPM driver board, (G) custom boost converter, and (H) lithium polymer battery.

To demonstrate our approach in creating tetherless fluid-powered soft robots, this paper focuses on an example case-study: a soft robotic fish (see Fig. 1). One common way fish achieve forward swimming is by composite caudal fin, peduncle, and body movement [2]. Motion in the fish's tail elegantly sheds vortices forming a jet with high propulsive efficiency [17] [18]. To emulate such motion, many electromechanical robotic fish utilize several actuators to drive joints within a multi degree-of-freedom tail. MIT's Robotuna utilizes six, 3 horsepower servomotors in its six DOF tail [4] [3]. G9, a robotic fish developed at the University of Essex, employs a

4 DOF tail [12] and NAF-I utilizes one passive and two active joints [22]. However, because of supporting hardware requirements, we do not yet have the capabilities to drive more than a single fluidic elastomer actuator onboard our robotic platform.

To meet the constraints of having a limited number of available actuators, but needing a wave-like motion, this paper develops an underactuated caudal fin and peduncle requiring only a single, bi-directional FEA, a locomotion scheme which can be realistically integrated within our soft robotic fish. We base our initial fin design on findings from [15], where a single electromechanical actuator was used to drive a compliant caudal fin. Considering the well documented hydrodynamic complexity of fish locomotion [19] [5] [10], we attempt to experimentally characterize various underactuated fish tail designs and control policies.

In the following sections, we present the design, implementation, and experimental verification of this novel, self-contained, fluidic robotic system and its propulsion system. Section 2 individually details the five major subsystems of the platform and their function within the aggregate system. Section 3 details experimental methodology and results used to verify critical aspects of system functionality. Lastly, section 4 explores major experimental insights.

2 Technical Approach

There are several enabling subcomponents of the self-contained fluidic actuation system. These subcomponents allow the system to simultaneously generate and regulate actuator supply pressure and control the deformation of FEAs.

In short, CO_2 is released from a high pressure (800 psi) canister to generate low driving pressure (3.5 psi) in an elastic reservoir. Miniature control valves allow gas to deplete from the reservoir into actuators and govern actuator pressurization.

2.1 CO_2 Storage and Release Mechanism

Detailed in Fig. 2 (A), this component houses an 8 gram CO_2 canister (I) punctured by a commercially available trigger valve (K). Valve displacement, and correspondingly CO_2 release, is controlled by a linear voice coil (J). To facilitate trigger valve actuation under onboard power constraints, a preload spring (L) is employed.

2.2 Elastic Reservoir Vessel

Detailed in Fig. 2 (B), this spherical, thick-walled silicone elastic vessel is filled with gas by A and depleted of gas by running the actuators, (D). Past a certain internal volume, pressure within the vessel remains relatively constant independent of volume changes. Such vessel design is highly advantageous in driving a FEA: air may leave the vessel and enter the actuators while the vessel passively maintains constant driving pressure and alleviates the system from continually replenishing the reservoir.

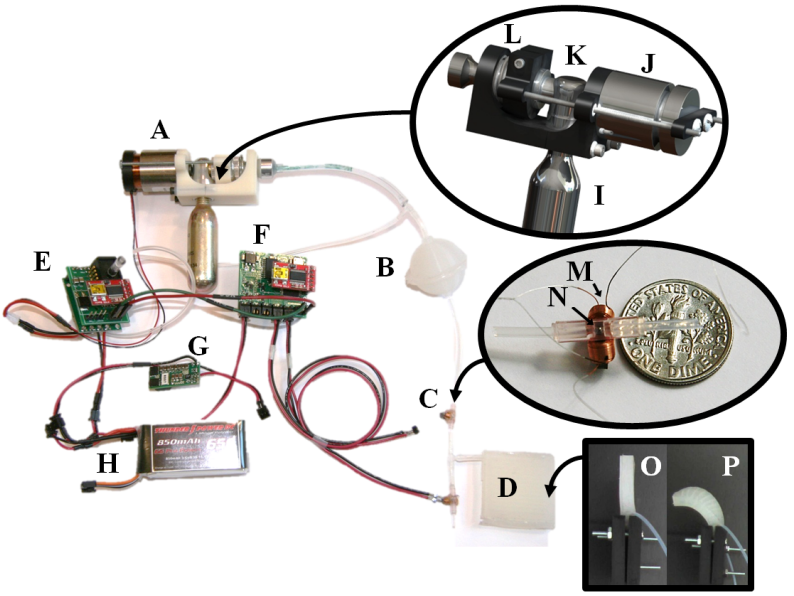

Fig. 2 Self-contained fluidic actuation system. The system is composed of (A) CO_2 storage and release mechanism, (B) elastic reservoir vessel, (C) embeddable electro-permanent magnet (EPM) valves [13], (D) fluidic elastomer actuator [7, 14, 13], (E) custom CO_2 regulator board, (F) custom EPM driver board, (G) custom boost converter, and (H) lithium polymer battery.

2.3 Electropermanent Magnet (EPM) Valves

Detailed in Fig. 2 (C), these embeddable control valves are a vast improvement both in size and energy consumption on the authors' previous work [13]. These valves turn ON and OFF gas flow with only a momentary pulse of energy (8 ms, 5 A) through coils (M) surrounding hard magnetic material and require no input energy to indefinitely maintain a state. A pulse either establishes or cancels a magnetic field in a fluidic channel, moving a small steel ball (N) away from or towards a sealing orifice.

2.4 Control Circuitry

Detailed in Fig. 2 (E and F). E measures elastic vessel (B) internal pressure as feedback for a bang-bang control routine used to drive the linear voice coil (J). F drives EPM valves (C) by controlling input current pulse duration and direction. E suppresses F when pressure drops below threshold and the reservoir is being filled.

2.5 *Underactuated Caudal Fin and Peduncle*

The caudal fin and peduncle were designed to meet the functional objective of producing forward thrust while meeting the constraint of being driven by a single bi-directional FEA, detailed in Fig. 2 (D). The actuator is shown in a restored, or depressurized state (O) and in a fully displaced, or pressurized state (P). Fig. 3 details the fabricated underactuated caudal fin (A) and peduncle (B) system. The compliant caudal fin is cut from 10 mil PEEK (Polyether ether ketone) film and is secured to the elastomer actuator using 2-56 nylon machine screws (C). The constraining (center) layer of the actuator is also composed of PEEK material and acts to quickly return the elastomer actuator to its restored state during depressurization. The actuator is cast from ECOFLEX 0030 silicone rubber.

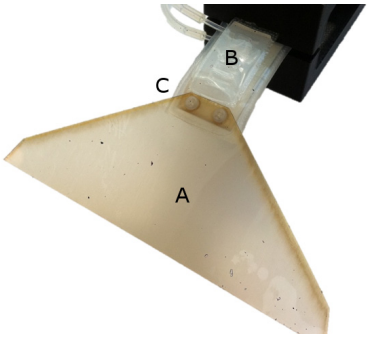

Fig. 3 Underactuated caudal fin (A) and peduncle (B). The caudal fin is composed of a thin PEEK material and joined to the peduncle, a fluidic elastomer actuator (FEA), through small screws at (C).

3 Results

Figure 4 displays top-view snapshots of our prototype system during operation. In this experiment, all sub-components are assembled and programmed to work together to verify system functionality. An elastic reservoir vessel acts as a passive pressure regulator for the high-pressure CO_2 cartridge and EPM valves drive a fin-shaped bidirectional FEA at 1 Hz.

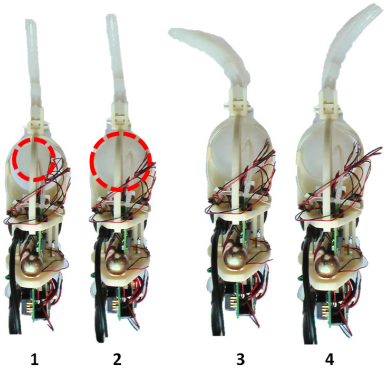

Fig. 4 The fluidic actuation system is used to realize natural, fish-like motion. In (1) the elastic reserve vessel (red-dashed circle) is uninflated. In (2) the reserve vessel is inflated with CO_2 gas. The right and left sides of the fin shaped bidirectional fluidic elastomer actuator are pressurized, curving the fin to the left (3) and right (4) sides, respectively.

3.1 Fluidic Actuation System Performance

Fig. 5 depicts the system regulating supply pressure, P_{sup}, (blue) between a reference (dashed line) and threshold (solid line) in the presence of actuator pressurization and depressurization (red) at 1 Hz. Time period (A) represents the CO_2 valve initially opening, (B) gas filling the elastic vessel (3 seconds), (C) CO_2 valve closing (0.5 seconds), and (D) the elastic pressure vessel maintaining a relatively constant supply pressure while EPM control valves drive rapid actuation. Event (F) represents initial pressurization of the system and event (E) the initial passive closure of the EPM control valves. Pressure is sampled at 50Hz.

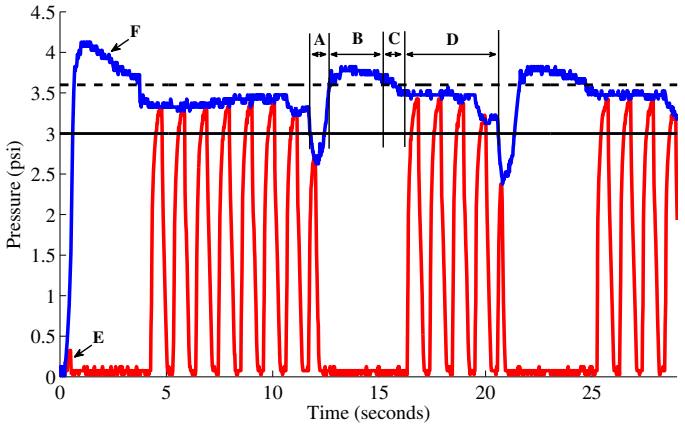

Fig. 5 Fluidic actuation system generating and regulating supply pressure (blue curve) between a reference (dashed line) and threshold (solid line) in the presence of actuator pressurization and depressurization (red curve). As the actuator depletes reservoir volume, properties of the elastic vessel passively regulate supply pressure and enable infrequent CO_2 valve actuation.

The fluidic actuation system was run according to the following algorithm:

Algorithm 1. Control Algorithm for Fluidic Actuation System

$Error = Reference - P_{sup}$
if $Error < Threshold$ and valve is closed **then**
  CO_2 valve idle
end if
if $Error \geq Threshold$ and valve is closed **then**
  (1) Suppress actuation, (2) Open CO_2 valve
else
  (1) Close the valve, (2) Unsuppress actuation
end if

Table 1 summarizes the system running for an extended duration of time. Here, a single fluidic actuator was driven at 1 Hz under the pressurization characterized in Fig. 5. Elastic vessel fill volume was varied from test 1 to test 2 and adjusted prior to running the system.

Table 1 Measured system parameters during extended operation

Test	Duration	Vessel Fills	Actuations	Charge Consumed	Gas Consumed
1	184[a] (sec)	20	85	96 (mAh)	1080[b] (mL)
2	180[a] (sec)	20	65	127 (mAh)	880[b] (mL)

[a] Test terminated due to excessive heating of boost converter.
[b] Estimate from average vessel expansion (1.9 and 1.8 in. respectively).

The pressure-volume relationship within the reservoir is highly non-linear. Initially, as volume within the vessel increases, pressure increases. However, past a certain internal volume (15 mL), pressure within the vessel remains relatively constant independent of volume changes. This "plateau pressure" is proportional to vessel wall thickness and is experimentally characterized in Fig. 6. Here, volume was manually injected into vessels of varying wall thickness (0.125, 0.25, and 0.375 in.) using a 60 mL capacity syringe in 2 mL increments up to 20 mL and 10 mL increments up to 40 mL. At each volume corresponding gauge pressure measurements were collected.

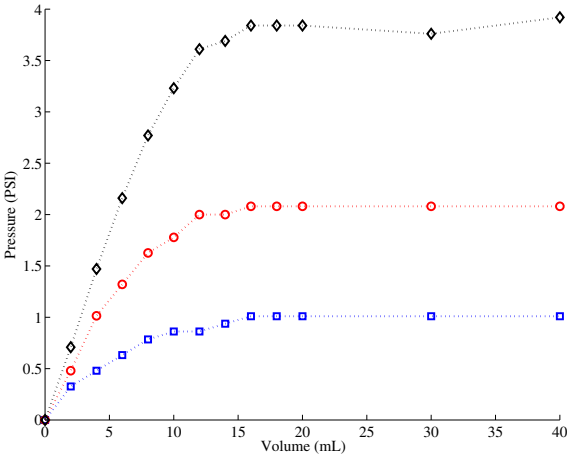

Fig. 6 The reserve vessel's internal pressure remains relatively constant independent of volume changes past a specific volume increase (15 mL). This "plateau pressure" is proportional to the vessel's wall thickness. Black represents a wall thickness of 0.375 in., red 0.25 in., and blue 0.125 in. In all vessels, O.D. was initially 1.25 in.

3.2 Underactuated Caudal Fin and Peduncle Performance

3.2.1 Experimental Setup

In order to evaluate the static thrust produced by a variety of caudal fin and peduncle combinations under various control policies in a controlled setting, the experimental assembly detailed in Fig. 7 was fabricated. The purpose of this assembly was to suspend a robotic fish tail and fin (A) vertically in a tank of water (50.8 cm long, 25.4 cm wide, 30.5 cm high) and measure the resulting stationary thrust force of a given control policy through a force transducer (C), (LSB200 2 lb Cap, FUTEK Advanced Sensor Technology, Inc.). Supports were fabricated to both secure the tail to the force transducer (B) and secure the entire described apparatus to the walls of the water tank (D). A similar vertical experimental setup was used in a paper detailing the effects of caudal fin compliance on propulsive force [15].

The amplified force transducer signal was acquired at 500Hz using a USB-6211 DAQ (National Instruments). In software, the force signal was zeroed prior to running a policy and, after a stabilization period, averaged over three policy-dependent cycle periods. Fig. 8 (a) details the force signal over three periods for a control policy resulting in net thrust. An average negative force is produced corresponding to transducer compression or vertical thrust force. Additionally, pressure inside both sides of the fluidic elastomer actuator was measured using two ASDX series 15 psi differential pressure transducers (Honeywell Sensing and Control). Fig. 8 (b) details the corresponding pressure profile for the above referenced control policy. Furthermore, two control valves (100 psi, 2 watt, 411 series, ASCO) were used to pressurize and depressurize each side of the bi-directional actuator (four control valves total). The valve array was driven by a custom embedded controller responsible for realizing policies, detailed in Sec. 2.4. Policies were communicated from a host PC to the low level embedded controller through a MATLAB serial communication interface.

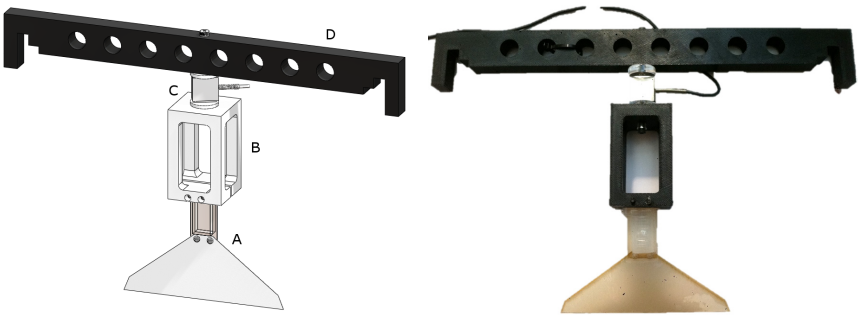

(*a*) (*b*)

Fig. 7 Experimental setup used to measure the static thrust produced by various control policies for various caudal fin and peduncle combinations. The apparatus consists of a force transducer (C) secured to the vertically suspended fish tail (A) through a support at (B). A second support (D) suspends the entire apparatus vertically in a tank of water.

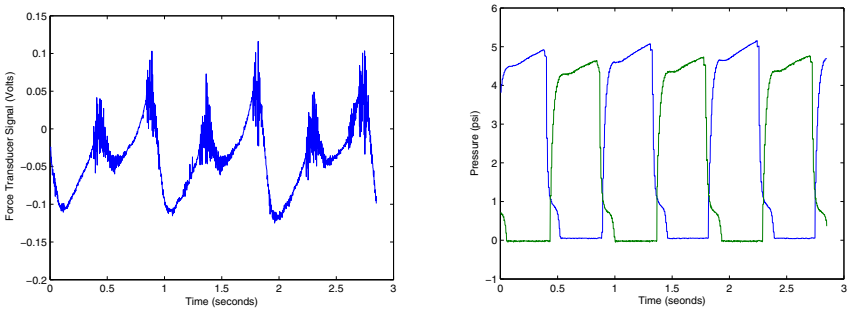

(a) (b)

Fig. 8 Transducer compressive or vertical thrust force signal profile over three strokes of a control policy resulting in a net thrust (a) and internal elastomer actuator pressure profile over the same time period (b)

3.2.2 Policy Parametrization

Control policies were parameterized using as few variables as possible. Fig. 9 details policy parametrization. A policy, α, consists of four time periods, T1 - T4, which when summed define one cycle of a periodic stroke. T1 is the pressurization time of the right elastomer actuator segment, and is realized by closing the right actuator's outlet valve and opening the inlet valve. When the right actuator pressurizes, the peduncle curves to the left. T2 is the depressurization time of the right elastomer actuator, and is realized by closing the actuator's inlet valve and opening the outlet. At the onset of depressurization, the peduncle begins to return to its restored state. T3 and T4 represent identical time periods for the left actuator. Policies were realized with 1 ms precision. A minimum of 25 ms was imposed on T1-T4, as this corresponds to the fastest realizable switching frequency of the solenoid valves. A maximum was empirically determined for each actuator to avoid damaging elastomer channels.

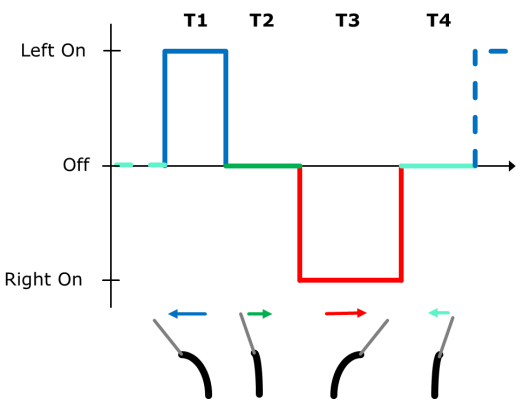

Fig. 9 Control policies, α, were parameterized using pressurization and depressurization times of the bidirectional actuator. T1 and T2 correspond to the pressurization and depressurization times of the left-side actuator and T3 and T4 to the right-side actuator, respectively. These four times constitute one cycle of a periodic stroke.

3.2.3 Test Scenarios

A total of 64 tests were conducted. Two FEAs, or peduncles, were evaluated: small measuring 1.27 by 2.54 by 0.95 centimeters and large measuring 2.54 by 2.54 by 0.95 centimeters. Two fin areas were evaluated: small measuring 15.5 and large measuring 32.1 square centimeters. Two control strategies were evaluated, active depressurization and passive depressurization. During active depressurization, T2 and T4 were held at control limit minimums (25 ms) allowing the pressurization of one side of the bidirectional FEA to forcefully depressurize the other side. During passive depressurization, T2 and T4 were equal to T1 and T3 allowing each side of the FEA sufficient time to depressurize before the other is pressurized. Lastly, pressurization times, T1 and T3, were set equal and varied incrementally from either 83 or 142 ms (depending on depressurization strategy) to 450 or 750 ms (depending on actuator size limitations).

During each scenario **static force (F)**: the average thrust force over three oscillations after a stabilization period, **wake (W)**: double fin oscillation amplitude, and **Pressure (P)**: mean peak internal actuator pressure after stabilization were calculated. In addition, **efficiency** was estimated for each scenario as: $\frac{F}{6T_1 P\dot{V}}$ in milliNewtons per unit of input energy, where $\dot{V}$ is an estimated volumetric flow rate and is constant for all scenarios.

Fig. 10 details the frequency wake product as a function of the system's control input, pressurization time, for the small actuator. In general, independent of fin area or depressurization strategy, the frequency-wake product increased with pressurization time. However, as expected the product begins to plateau as both oscillation amplitude and frequency plateau with linear increases in pressurization time.

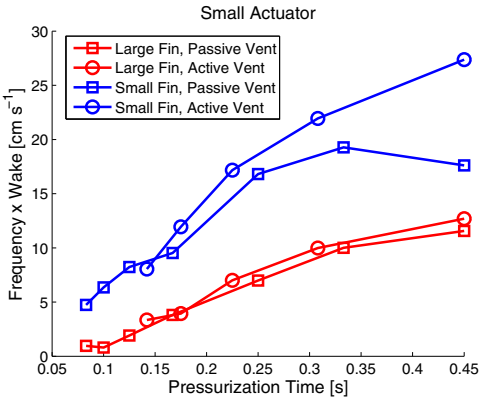

Fig. 10 Frequency-wake product as a function of the system's control input, pressurization time, for the small actuator. Here, red and blue represent large and small fin areas respectively and squares and circles represent passive and active depressurization (vent) strategies respectively.

Fig. 11 details the stationary thrust produced as a function of frequency-wake product for the small actuator. In general, independent of fin area or depressurization strategy, the thrust force increased near-exponentially with frequency-wake product.

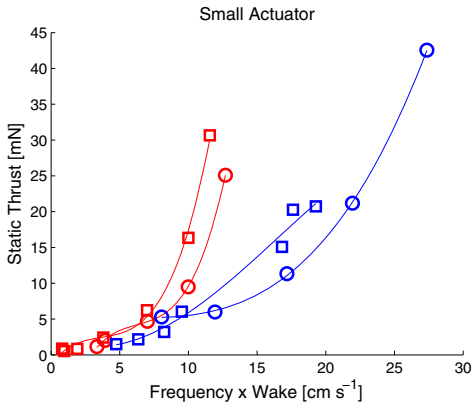

Fig. 11 Stationary thrust produced as a function of frequency wake product for the small actuator

Furthermore, Fig. 12 details the estimated efficiency, or output force per unit input energy, as a function of the frequency-wake product for the small actuator. In general, a higher product resulted in greater efficiency.

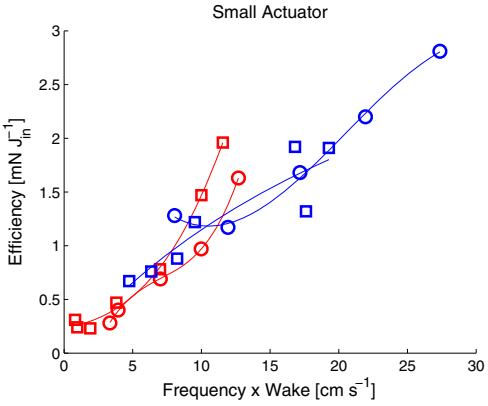

Fig. 12 Estimated efficiency, or output force per unit input energy, as a function of the frequency-wake product for the small actuator

Fig. 13 details both the frequency-wake product as a function of pressurization time and stationary thrust force as a function of frequency-wake product for the larger actuator. In general, the results are similar to the the smaller actuator; however, a notable difference is that during a passive depressurization strategy (squares) the larger actuator's ability to generate thrust decreases past a certain frequency-wake product. We believe this is due to longer than necessary depressurization times creating a sudden decrease in fin velocity during the stroke. Essentially, when one side of the actuator depressurizes, the fin returns to its neutral, restored state, and if the fin reaches this restored state before the alternate actuator side begins to pressurize the fin can be slowed to a stop in the middle of a stroke.

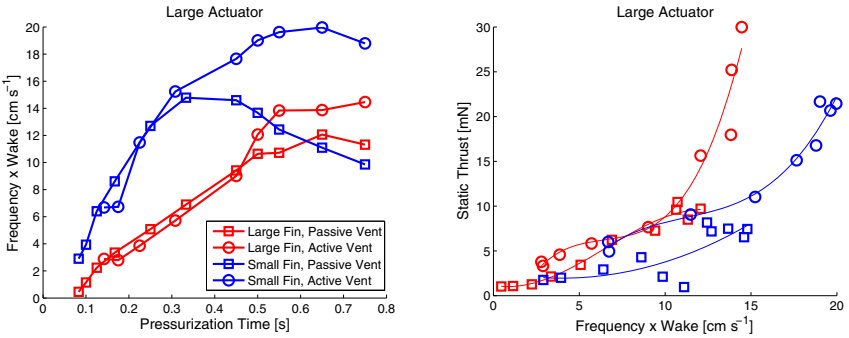

Fig. 13 Frequency-wake product as a function of pressurization time and stationary thrust force as a function of frequency-wake product for the large actuator

4 Main Experimental Insights

EPM Valve Efficiency. During experiments in Table 1, an 8 ms pulse of 5 A was used to drive the EPM control valves. Two valves were used at the inlet and outlet of the single actuator, and 4 pulses were required per actuation cycle. In test 1, the valves consumed an estimated 3.8 mAh during the 85 actuations, a mere 4% for the total energy consumed. In test 2, estimated EPM energy consumption amounted to 2.3%

CO_2 Capacity Limits. Using Van der Waals non ideal gas equation, the maximum theoretical volume available in the system is 3.5 Liters.

$$\left(p + \frac{n^2 a}{V^2}\right)(V - nb) = nRT \tag{1}$$

Where, p is the supply pressure (0.125 MPa), T gas temperature (296 K), R gas constant, n number of moles (0.182), a measure of attraction between particles (0.364 $\frac{Jm^3}{mol^2}$), and b volume excluded by a mole of particles (0.00004267 $\frac{m^3}{mol}$).

Reservoir Fill Volume. As the results in Table 1 indicate, for the same duration of time a larger periodic fill volume allows the system to spend more time operating the fluidic elastomer actuators and expend less energy opening and closing the CO_2 valve.

Underactuated Caudal Fin and Peduncle. As is shown in the experimental results, pressurization time provides control authority, though limited, over frequency-wake product and correspondingly stationary force generation. Physical limitations on pressurization time and frequency-wake coupling inhibit arbitrarily large frequency wake products.

Considering only the active depressurization strategy scenarios, with the larger fin area both the small and large actuators had the same average efficiency 0.79 $\frac{mN}{J_{in}}$.

However, with the smaller fin area the small actuator was almost twice as efficient as the larger actuator with average efficiencies of 1.83 and 1.13 $\frac{mN}{J_{in}}$ respectively.

Many researchers have thoroughly investigated the propulsive efficiency of flapping foils in a *dynamic* setting [11] [16] [17]. For these studies, efficiency and thrust coefficients of oscillating foils were determined as a function of Strouhal number, a critical parameter describing vortex pattern formation behind moving foils, and a parameter that is dependent on, among other quantities, stream/body velocity. This current analysis is limited to zero body velocity, so we cannot assume any of the same underlying hydrodynamic phenomena (i.e. reverse Karman street) are at work.

Acknowledgements. This work was done in the Distributed Robotics Laboratory at MIT with partial support from the DARPA DSO "Chembots" project (W911NF-08-C-0060), the Boeing Company, and the National Science Foundation Graduate Research Fellowship Program, Primary Award #1122374. We are grateful for this support.

References

1. Albu-Schaffer, A., Eiberger, O., Grebenstein, M., Haddadin, S., Ott, C., Wimbock, T., Wolf, S., Hirzinger, G.: Soft robotics. IEEE Robotics & Automation Magazine 15, 20–30 (2008)
2. Bainbridge, R.: Caudal fin and body movement in the propulsion of some fish. Journal of Experimental Biology 40, 23–56 (1963)
3. Barrett, D.S.: Propulsive efficiency of a flexible hull underwater vehicle. Ph.D. thesis, Massachusetts Institute of Technology, Cambridge, MA, USA (1996)
4. Barrett, D.S., Triantafyllou, M.S., Yue, D.K.P., Grosenbaugh, M.A., Wolfgang, M.J.: Drag reduction in fish-like locomotion. Journal of Fluid Mechanics 392, 183–212 (1999)
5. Borazjani, I., Sotiropoulos, F., Tytell, E.D., Lauder, G.V.: Kinematics and muscle dynamics of C- and S-starts of carp (Cyprinus carpio L.). Journal of Experimental Biology 215, 671–684 (2012)
6. Calisti, M., Giorelli, M., Levy, G., Mazzolai, B., Hochner, B., Laschi, C., Dario, P.: An octopus-bioinspired solution to movement and manipulation for soft robots. Bioinspiration & Biomimetics 6(3), 036,002 (2011)
7. Correll, N., Önal, Ç.D., Liang, H., Schoenfeld, E., Rus, D.: Soft autonomous materials—using active elasticity and embedded distributed computation. In: Khatib, O., Kumar, V., Sukhatme, G. (eds.) Experimental Robotics. STAR, vol. 79, pp. 227–240. Springer, Heidelberg (2012)
8. Kazerooni, H.: Design and analysis of pneumatic force generators for mobile robotic systems. IEEE/ASME Transactions on Mechatronics 10(4), 411–418 (2005)
9. Knaian, A.N.: Electropermanent magnetic connectors and actuators: devices and their application in programmable matter. Ph.D. thesis, Massachusetts Institute of Technology, Cambridge, MA, USA (2010)
10. Lauder, G., Lim, J., Shelton, R., Witt, C., Anderson, E., Tangorra, J.: Robotic models for studying undulatory locomotion in fishes. Marine Technology Society Journal 45(4), 41–55 (2011)
11. Licht, S., Polidoro, V., Flores, M., Hover, F., Triantafyllou, M.: Design and projected performance of a flapping foil auv. IEEE Journal of Oceanic Engineering 29(3), 786–794 (2004)

12. Liu, J., Hu, H.: Biological inspiration: From carangiform fish to multi-joint robotic fish. Journal of Bionic Engineering 7, 35–48 (2010)
13. Marchese, A.D., Onal, C.D., Rus, D.: Soft robot actuators using energy-efficient valves controlled by electropermanent magnets. In: 2011 IEEE/RSJ International Conference on Intelligent Robots and Systems (IROS), pp. 756–761 (2011)
14. Onal, C.D., Chen, X., Whitesides, G.M., Rus, D.: Soft mobile robots with on-board chemical pressure generation. In: International Symposium on Robotics Research, ISRR (2011)
15. Park, Y.J., Jeong, U., Lee, J., Kim, H.Y., Cho, K.J.: The effect of compliant joint and caudal fin in thrust generation for robotic fish. In: 2010 3rd IEEE RAS and EMBS International Conference on Biomedical Robotics and Biomechatronics (BioRob), pp. 528–533 (2010)
16. Schouveiler, L., Hover, F., Triantafyllou, M.: Performance of flapping foil propulsion. Journal of Fluids and Structures 20(7), 949–959 (2005)
17. Triantafyllou, G., Triantafyllou, M., Grosenbaugh, M.: Optimal thrust development in oscillating foils with application to fish propulsion. Journal of Fluids and Structures 7(2), 205–224 (1993)
18. Triantafyllou, M., Triantafyllou, G.: An efficient swimming machine. Scientific America 272(3), 64–70 (1995)
19. Triantafyllou, M., Triantafyllou, G., Yue, D.K.: Hydrodynamics of fishlike swimming. Annual Review of Fluid Mechanics 32, 33–53 (2000)
20. Trivedi, D., Rahn, C., Kier, W., Walker, I.: Soft robotics: Biological inspiration, state of the art, and future research. Advanced Bionics and Biomechanics 5(2), 99–117 (2008)
21. Wait, K., Jackson, P., Smoot, L.: Self locomotion of a spherical rolling robot using a novel deformable pneumatic method. In: 2010 IEEE International Conference on Robotics and Automation (ICRA), pp. 3757–3762 (2010)
22. Zhong, Y., Chong, C., Zhou, C., Seet, G., Low, K.: Performance predict model for a body and caudal fin (bcf) biomimetics fish robot. In: IEEE/ASME International Conference on Advanced Intelligent Mechatronics, AIM 2009, pp. 1230–1235 (2009)